A Deep Learning-Monte Carlo combined prediction of side-effect impact ionization in highly doped GaN diodes

S. García-Sánchez, R. Rengel, S. Pérez, T. González, *Senior Member, IEEE*, and J. Mateos, *Member, IEEE*

Abstract - The existence of leakage current pathways leading to the appearance of impact ionization and the potential device breakdown in planar Gunn GaN diodes is analyzed by means of a combined Monte Carlo-deep learning approach. Front-view (lateral) Monte Carlo simulations of the devices show the appearance of a high-field hotspot at the anode corner of the etched region, just at the boundaries between the dielectric, the GaN-doped layer, and the buffer. Thus, if the isolation created by the etched trenches is not complete, a relevant hot carrier population within the buffer is observed at sufficiently high applied voltages, provoking the appearance of a very significant number of impact ionizations and the consequent avalanche process before the onset of Gunn oscillations. A neural network trained from Monte Carlo simulations allows predicting with extremely good precision the breakdown voltage of the diodes depending on the doping of the GaN active layer, the permittivity of the isolating dielectric, and the lattice temperature. Low doping, high temperature and high permittivity provide larger operational voltages, which implies a tradeoff with the conditions required to achieve THz Gunn oscillations at low voltages.

Index Terms— Gunn diodes, doped GaN, THz generation, Monte Carlo simulations, electronic transport, artificial intelligence (AI), deep learning.

I. Introduction

Terahertz (THz) waves have attracted a great interest in the last decade, but the lack of powerful sources has hindered the spreading of practical applications using this region of the electromagnetic spectrum. In order to try to fill up the so-called THz gap, different aproaches are used, from low temperature gas and quantum cascade lasers to bulky and complex setups based on laser driven photomixers or free electron based sources, but the preferred approach is the use of electronic solid state sources [1], [2]. Despite of huge efforts made in recent years, there is still a lack of compact and portable THz sources based on solid-state devices able to operate at room temperature. Some solutions have been explored in the literature: frequency multipliers based on GaAs Schottky diodes have demonstrated decent output power performances in the mm and sub-mm wave ranges: 139 μW@1.6 THz and 32 μW@2.4 THz [3] 125 mW in the 270-300 GHz frequency range [4], all of them based on amplified low-frequency (below 50 GHz) fundamental oscillators. Another possible solution to generate frequencies in the THz range is the utilization of active two-terminal devices, exploiting a negative differential resistance (NDR), to fabricate high power fundamental oscillators at frequencies above 100 GHz, which may be multiplicated afterwards. Devices that are relevant at submillimeter waves are resonant-tunnelling diodes (RTDs), tunnel injection transit-time devices (TUNNETT), super lattice electronic devices (SLEDs) and transferred-electron devices (TEDs, also called Gunn devices) [5]. Focusing on the latter, vertical InP Gunn devices in a third-harmonic mode yielded 330 mW@412 GHz and 86 mW@479 GHz at 300 K [5]. Also, planar Gunn diodes (PGDs) fabricated on $In_{0.53}Ga_{0.47}As$ have been demonstrated, providing 28 μW@307 GHz [6]. However, the small bandgap of such GaAs and InP based semiconductors is an intrinsic limitation for increasing the generated power. That is why with the recent advances in the growth of high quality GaN, thanks to its large bandgap and reasonable NDR, this semiconductor is becoming a promising candidate for the fabrication of high-power high-frequency Gunn diodes Simulations of GaN-based diodes indicate the possibility of achieving Gunn oscillations with frequencies above 500 GHz, faster than in traditional semiconductors due to the short relaxation time of GaN [7]-[12]. Furthermore, the NDR of GaN has been observed and indirect evidence of current oscillations has been obtained [13]-[15], which allows us to believe on the practical feasibility of high-power high-frequency GaN Gunn diodes. Monte Carlo (MC) simulations have been used to design optimized device geometries for the fabrication of PGDs using shaped nanochannels, both based on AlGaN/GaN heterojunctions [16], [17] and highly doped GaN epilayers [18]-[21]. However, reliability problems arise due to the very high applied voltages needed to operate the diodes, such as electromigration in the ohmic contacts and catastrophic self-heating effects [14].

Improvements of the technology have been achieved [13] in order to avoid the diode failure by means of field plates and mesas with reduced area, but continuous DC operation is not possible yet. MC simulations show that well designed PGDs using shaped channels [17] are also able to avoid such undesirable effects by (i) focusing the electric field far from the contacts and (ii) limiting the amount of the dissipated DC power, but in that case impact ionization avalanche may appear as a destructive mechanism. Another advantage of PGDs is that

Manuscript received ¿? 2023; revised ¿? 2023; accepted ¿? 2023. Date of publication ¿? 2023; date of current version ¿? 2023.This work has been partially supported through grant PID2020-115842RB-I00 funded by MCIN/AEI/10.13039/501100011033.

S. García-Sánchez, R. Rengel, S. Pérez, T. González and J. Mateos, are with the Applied Physics Department, and USAL-NANOLAB, Universidad de Salamanca, Salamanca, Spain.

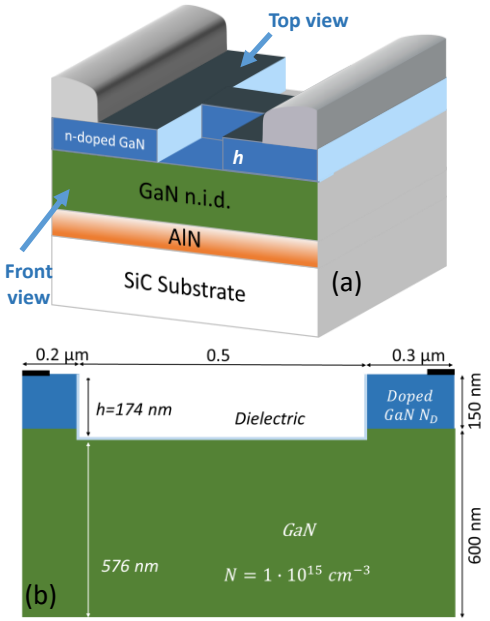

Fig. 1. (a) 3D structure of the simulated device. (b) Front-view of a longitudinal cut at the etched sides of a channel with an isolation depth of *h*=174 nm.

the technological process for its fabrication is very simple, just needing (apart from the ohmic contact fabrication) a single lithographic step to define the channels and the mesa, and its integration with planar antennae for the free-space coupling is straightforward.

MC studies of shaped nanochannels are based on a top-view modelling of the diodes, which is adequate to capture the main features of electronic transport in the doped or undoped GaN channel, and in particular, the formation of Gunn domains and the generation of THz waves. However, such approach does not account for the possibility of secondary transport paths in the underlying undoped GaN buffer (see Fig.1). In such devices, the highest electric fields appear at the anode end of the channel, at the corner of the etched regions. This would be unimportant if there is no transport through the buffer, but at the high biases needed for the generation of Gunn oscillations, high vertical fields force the electrons to penetrate into the undoped region. Consequently, some hot carriers, susceptible of provoking impact ionizations, can appear, thus leading to avalanche and the potential failure of the device [22]. Besides, defects and impurities could play a role in the appearance of tunneling leakage current in other types of GaN-based diodes [23], [24], but in the case of the planar diode architecture studied here, they are mainly effective at low electron energies, and do not have a significant influence.

In this work we present a front-view study of PGDs with the aim of analyzing the appearance of secondary transport channels and the onset of impact ionization phenomena. For this purpose, a combined MC-deep learning approach has been considered. First, front-view device MC simulations have been carried out to investigate the high energy region at the anode end of the channel, with particular focus on the appearance of hot electrons flowing through the buffer. Based on the results of the MC simulations, an Artificial Neural Network (ANN) has been trained to predict the device voltages that may lead to potential damage of the devices via impact ionizations. ANNs are being recently used in combination with different levels of simulations of technological processes, devices and circuits in order to develop and optimize semiconductor technologies by using physical (or compact) models [25]-[27].

The paper is organized as follows. In section II the main features of the simulated structures and the Monte Carlo model are described. In section III the results are presented and discussed, including the ANN model and predictions about the voltages to be applied to avoid significant impact ionization phenomena. Finally, the main conclusions are presented.

II. Monte Carlo Simulations and Device Details

A home-made semi-classical ensemble MC tool self-consistently coupled to a two-dimensional (2D) Poisson solver is employed for the simulation of electronic transport. More details about the simulator can be found in [10], [18], [21], [28]. GaN semiconductor is modeled considering three non-parabolic spherical valleys for the conduction band, whose main parameters can be found in Refs. [11], [29]. Impact ionization has been introduced as a scattering mechanism by using the Keldysh approach [30]-[32], where the probability per unit time of having an impact ionization event is given by $P(\varepsilon) = S \cdot ((\varepsilon - \varepsilon_{th})/\varepsilon_{th})^k$ if $\varepsilon > \varepsilon_{th}$, where ε is the total energy of the specific carrier, ε_{th} is the threshold energy for impact ionization, and S and k are dimensionless parameters which determine the amount of impact ionization processes and the softness or hardness of the threshold. These parameters are taken as adjustable in order to reproduce the ionization coefficient of the simulated semiconductor. In this study, we have chosen the values ε_{th}=3.5 eV, S=10 ps^{-1} and k=4 because they provide a good agreement with the results of ref. [31], and lie within the range of the experimental values found in the literature [33], [34]. A surface charge σ is introduced at the interface between the dielectric and the semiconductor by using a self-consistent surface charge model (more details can be found in Ref. [35]), so that σ is updated self-consistently with the carrier dynamics near the interface during the simulations. Simulations were carried out by considering a time-step of Δt=0.2 fs for a total time of 40 ps.

The details of the simulated device are sketched in Fig. 1(b). The simulated structure corresponds to a front-view of a longitudinal cut within the isolated region of a PGD. The layer structure features a 150-nm-thick doped GaN layer grown on top of a 600 nm-thick undoped GaN buffer. We have to note that the buffer thickness in real epilayers would be larger in order to reduce the threading dislocation density, which can be a source of buffer leakage [36]. However, we chose a 600 nm thickness for the simulated structure since simulating a thicker epilayer would provide identical results, while increasing unnecessarily the computational cost. For the doped GaN region, doping levels in the range N_D=0.5-10×10^{18} cm^{-3} are studied. The structure has an etched region with a depth of 174 nm, filled with dielectrics with relative permittivity in the range κ_r=1-6. The device mesh discretization has been done by using 225 rows and 500 columns, having a total number of 112,500 cells.

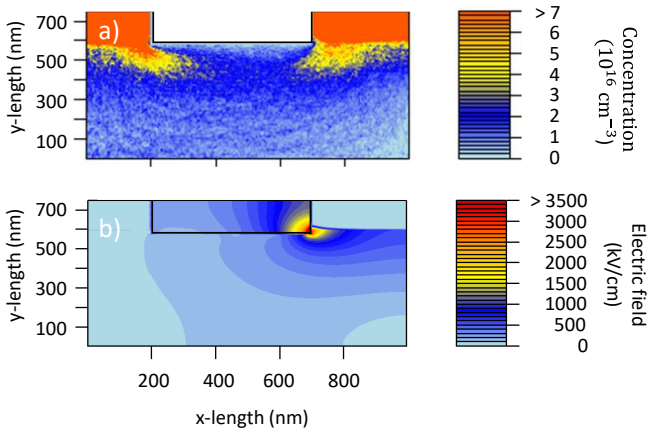

Fig. 2: Maps of (a) electron concentration and (b) module of the electric field for a bias of 26 V at 300 K. The doping of the active layer is N_D=5×10^{18} cm^{-3} and the relative permittivity of the dielectric (air) is κ_r=1.

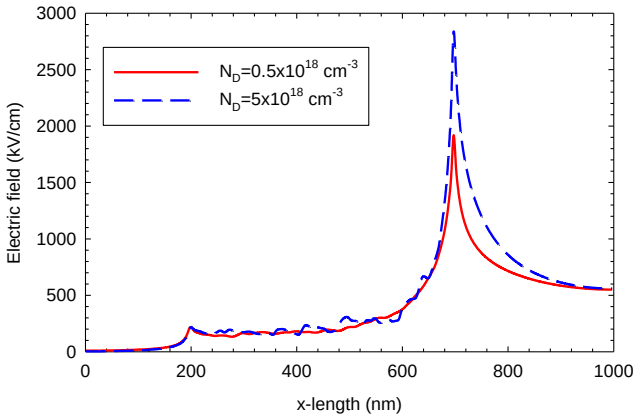

Fig. 3. Profile of the electric field at the y position of 574 nm for a bias of 26 V using κ_r=1 and N_D=0.5×10^{18} cm^{-3} and 5×10^{18} cm^{-3}.

III. RESULTS AND DISCUSSION

Fig. 2(a) shows the electron concentration for a bias of 26 V at 300 K, considering a relative permittivity κ_r=1 for the dielectric (air in that case) and a doping level of the doped GaN layer equal to 5×10^{18} cm^{-3}. As it can be observed, a remarkable electron penetration into the buffer layer takes place when a high bias is applied to the anode. This implies the appearance of unintended, secondary transport paths, that may play a significant role under the presence of high electric fields. Indeed, as shown in Fig. 2(b), the electric field displays a hotspot at the anode corner of the etched region, just at the boundaries between the dielectric, the GaN-doped layer and the buffer. The value of the electric field at this hotspot is influenced by the doping value of the doped GaN layer. Fig. 3 shows the profiles of the electric field at the y-position of 574 nm (just below the dielectric/semiconductor interface) for doping levels of 0.5 and 5×10^{18} cm^{-3}, reaching maximum values of 1.9 and 2.8 MV/cm respectively. It is then clear that a larger doping favours the increase of the electric field at such hotspot. We have to note here that this electric field crowding is less significant than that appearing at the anode contact edge in vertical Gunn diodes, where MC simulations show that the electric field can be much higher, so that field-plate strategies as the one shown in [13] are needed to avoid the device failure.

In order to analyse to which extent such high electric field hotspot is able to generate hot electrons, firstly the distribution function of the total energy (DFE) of electrons has been computed for each mesh. Fig. 4 shows the 50th and 99th percentiles of the total energy when biases of 16 and 26 V are applied (with T=300 K, κ_r=1 and N_D=5×10^{18} cm^{-3}). At 16 V, even if in a small area, at least 50% of the electrons around the hotspot region have energies higher than 3.5 eV (the threshold for impact ionization). Consequently, this region, which does not correspond to the primary transport path in this kind of device, can be identified as a potential area for the appearance of a relevant number of impact ionization events, that could potentially damage the diode. In fact, if one pays attention to the results for the carriers corresponding to the 99th percentile, i.e., the most energetic carriers, some even reach energies above 5.0 eV near the hotspot. The trajectories of some hot electrons through the buffer can also be clearly observed. This suggests that hot carrier side-effects, not identified in top-view studies of this type of diodes, can be of importance. At a larger voltage (i.e., 26 V), the same general trends are observed in Fig. 4 (d) and (e), but now the hot-carrier area, where impact ionization mechanisms could take place, is much broader. Also, the most energetic electrons can reach the bottom of the buffer. It is important to stress that, at the same time, carriers in the doped layer at the anode region remain with low energies.

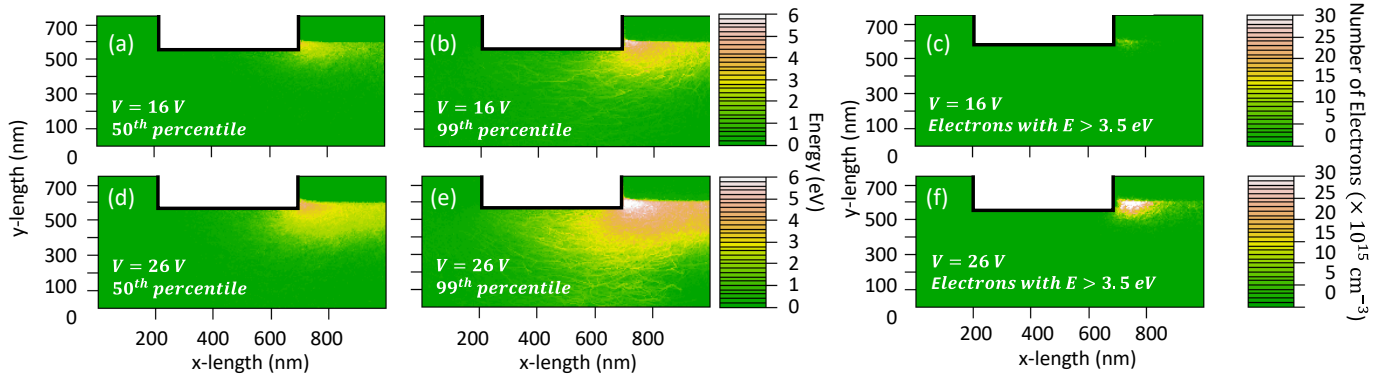

Fig. 4. Maps of percentiles of the total energy of electrons: (a) and (d) 50th and (b) and (e) 99th. (c) and (f) Show the concentration of electrons with total energy above 3.5 eV for T=300 K, κ_r=1 and N_D=5×10^{18} cm^{-3}. The top row corresponds to a bias of 16 V and the bottom to 26 V.

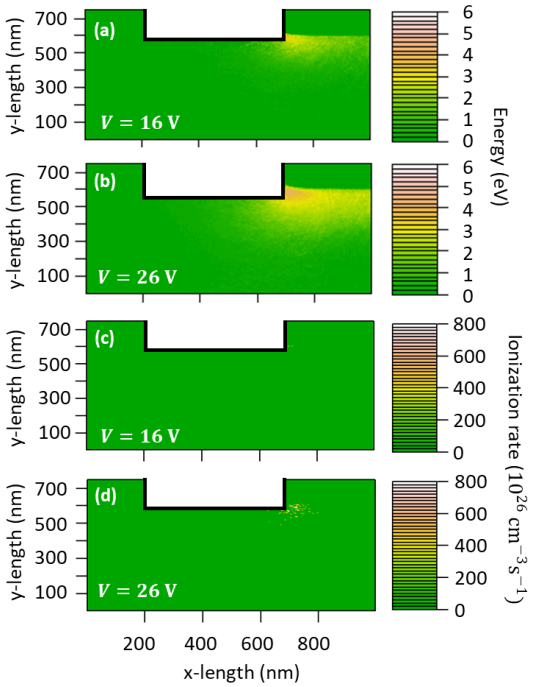

Fig. 5. Maps of (a) and (c) total energy of electrons and (b) and (d) ionization rate for T=300 K, κ_r=1 and N_D=5×10^{18} cm^{-3}. The top row corresponds to a bias of 16 V and the bottom to 26 V.

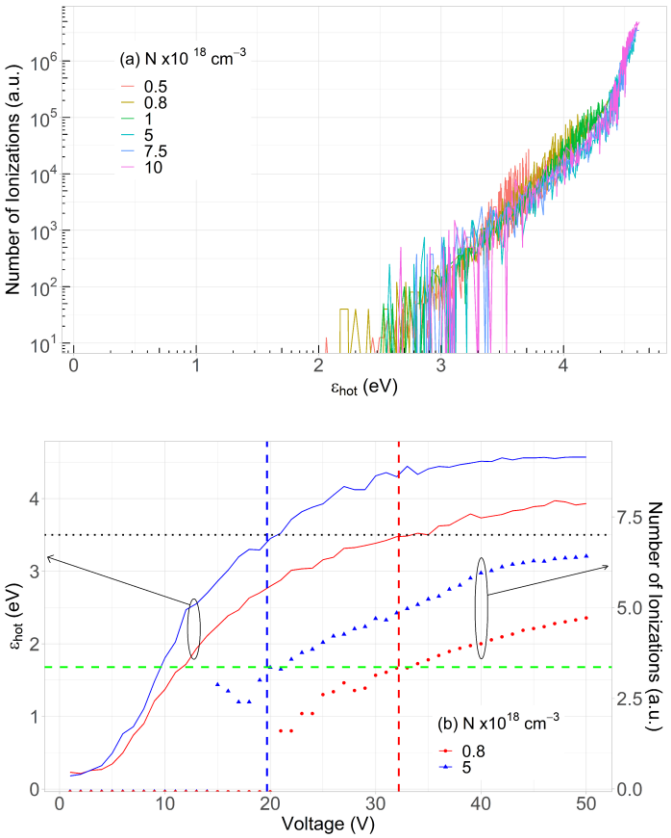

Fig. 6. (a) Total number of impact ionization events within the device plotted as a function of ε_{hot} for all the simulated values of N_D, T and κ_r. (b) Extraction of the value of V_B for two cases: (i) T=500 K, κ_r=6 and N_D=0.8×10^{18} cm^{-3} and (ii) T=300 K, κ_r=1 and N_D=5.0×10^{18} cm^{-3}.

To activate a breakdown mechanism, the existence of a high-field or a high electronic energy region must be accompanied by a relatively significant carrier concentration, which could trigger an impact-ionization avalanche process. In Figs. 4(c) and (f) we plot the concentration of hot electrons with energies larger than 3.5 eV (the impact ionization threshold energy ε_{th}), showing that only for V=26 V there is a significant number of electrons with those energies located beneath the doped GaN layer, while very few appear for V=16 V.

In order to avoid an excessive computation time, instead of the DFE we will use in a second step the average total energy as an indicator for the probability of appearance of impact ionization events. Let us note that the DFE has a right-skewed distribution and, accordingly, the value of the 50th percentile, ε_{50}, is lower than the average, ε_{av}. Indeed, if we compare the maps of ε_{av}, Figs. 5(a) and (b), with those of ε_{50}, Figs. 4(a) and (d), the information provided by both quantities is quite similar, just with slightly lower values for ε_{av}. Moreover, as seen in Fig. 5(c), impact ionization does not appear for V=16 V, as corresponds to electron average energies which hardly reach the threshold value of 3.5 eV. On the other hand, for V=26 V, ε_{av} reaches values above 4.0 eV, thus provoking the onset of frequent impact ionization events that would potentially lead to an avalanche process and device breakdown.

Once the threshold value of the energy for the impact ionization is evaluated, we will now choose a single parameter to identify whether or not the breakdown is likely to appear. For this sake, we define for a given applied voltage, the hot-spot energy, ε_{hot}. The value of ε_{hot} will be calculated by considering the 100 meshes (which represent less than 0.1% of the total meshes) with the highest total electron energy within the device. We have chosen this criterion based on the averaging of the energy of the hot-spot region, because it is statistically more representative than choosing the value of just one individual mesh. Fig 6(a) shows the direct link between the total number of ionizations within the device and the value of ε_{hot} (with a

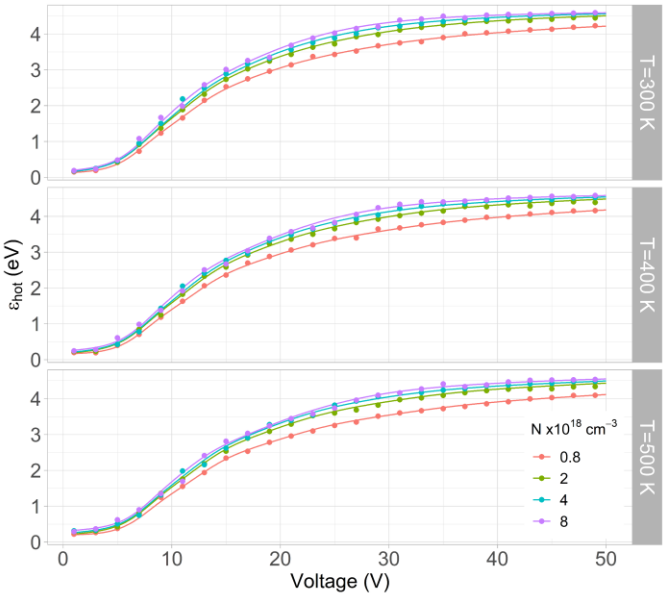

Fig. 7. ε_{hot} vs. applied voltage for lattice temperatures of 300, 400 and 500 K, κ_r=3 and N_D=0.8, 2.0, 4.0 and 8.0×10^{18} cm^{-3}. Solid lines correspond to results predicted from the ANN model and symbols to those from MC simulations.

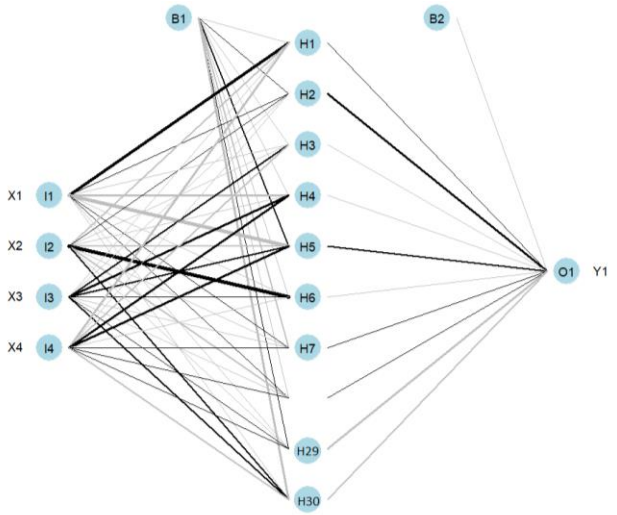

Fig. 8. Architecture of the ANN built. X_i: input variables (T, N_D and κ_r), I_i: input layer, H_i: hidden layer, O_1: output layer (ε_{hot}).

sharp exponential dependence), demonstrating that they are substantial when ε_{hot} reaches the threshold energy for the onset of impact ionization mechanisms (i.e., ε_{hot}=ε_{th}=3.5 eV). We will then estimate the voltage for which breakdown is expected, V_B, as the bias for which ε_{hot}=ε_{th}, as indicated in Fig. 6(b) for two extreme cases, one providing V_B below 20 V and the other above 30 V (one with low T, low κ_r and high N_D, and the other in the opposite range). In both cases the voltage for which ε_{hot} reaches the 3.5 eV threshold corresponds to the conditions where the number of impact ionizations starts to be significant. Fig. 7 shows the values of ε_{hot} obtained with the MC simulations as a function of the applied voltage under different conditions ranging from T=300 to 500 K and from N_D=0.8 to 8.0×10^{18} cm^{-3}, for κ_r=3. For example, in the two cases represented in Fig. 5, ε_{hot}=3.02 eV for V=16 V and 4.05 eV for V=26 V (below and above threshold, respectively).

Even if MC simulations provide this information in a natural way, as several quantities are considered as variable parameters, the number of simulations needed to provide an accurate estimation of ε_{hot} for every single case becomes prohibitive from the point of view of computational cost. To tackle this limitation and account for possible non-linear dependences with the different quantities involved, a model based on an ANN was considered. The developed model allows us making the prediction of ε_{hot} (the target variable), taking as input variables the applied bias, T, N_D and κ_r. In this way, for each combination of T, N_D and κ_r the breakdown voltage can be estimated from the voltage value that makes ε_{hot} reach the impact ionization threshold.

The ANN used features one hidden layer, which can approximate any function that contains a continuous mapping from one finite space to another, and it is an adequate choice for most problems [37], [38]. Regarding the size of the hidden layer, we have considered 30 neurons (Fig. 8) since we observed that this value provides a good fit on the training data as well as on new data. The neuralnet function from the package neuralnet in the R statistical software programming language [39] was used to implement the ANN, since this function uses resilient backpropagation method [40], [41], thus reducing the

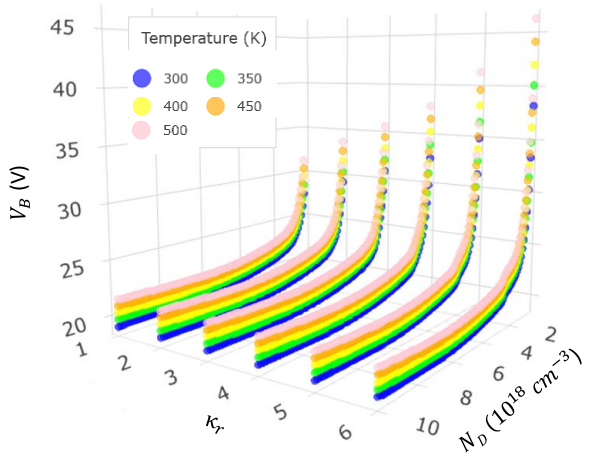

Fig. 9. Dependence of V_B with T, κ_r and N_D obtained with the ANN model.

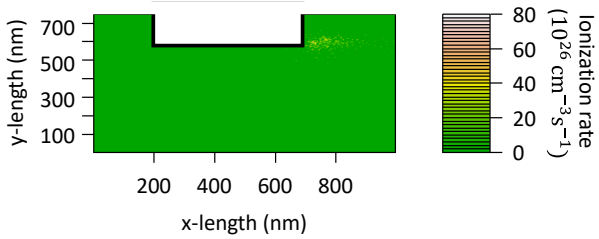

Fig. 10. Map of ionization rate for T=500 K, κ_r=6 and N_D=0.8×10^{18} cm^{-3} for an applied bias of 32.3 V.

cost function and fine-tuning the weights and thresholds of the ANN based on the error rate obtained in the previous iteration.

The model was validated by analysing the Mean Squared Error (MSE) loss function and the Mean Absolute Error (MAE) loss function [42]:

$$MSE = \frac{1}{N}\sum_{i}^{N}(y_i - \hat{y}_i)^2 \; ; \; MAE = \frac{1}{N}\sum_{i}^{N}|y_i - \hat{y}_i| \quad (1)$$

where N is the number of data points on all variables, y_i the observed value and $\hat{y}_i$ the predicted value. MSE should be interpreted as an error metric where the closer the value is to 0, the more accurate the model is. Also, the closer MAE is to 0, the more accurate the model is, but MAE is returned on the same scale as the target we are predicting. The maximum steps for the convergence criteria for training the NNET (*stepmax* parameter in the neuralnet function) has been configured to 10^{10}. Also, a Sigmoid or Logistic activation function has been used (*act.fct="logistic"*).

For the training process, we have used as data input the results of 972 MC simulations with applied voltages from 1 V to 50 V (with a non-homogeneous step in order to optimize the training), N_D from 0.5 to 10×10^{18} cm^{-3}, κ_r of 1, 3 and, 6, and T of 300, 400 and 500 K. After the training process, we validate our model by analyzing the MSE and MAE metrics for the data training and the data test (data not used in the training process). The MSE obtained are 1.7 and 2.3 meV^2, and the MAE are 0.036 and 0.031 eV, for training and test data respectively, which shows the good accuracy of the ANN to predict the values of ε_{hot}. It is important to remark that this procedure allows combining a very precise determination of the target variable with a huge reduction of the computational time as

compared to a full set of MC simulations. Each individual MC simulation takes a CPU time close to 48 hours in a computer cluster based on Intel Xeon 6234@3.3GHz processors. Therefore, the computing time employed for getting the training data (972 MC simulations) was equivalent to approximately 46,500 hours. However, training the ANN takes just a few minutes, and getting the results presented in Fig. 9 by using the developed model (which would involve 3,000 MC simulations, and 144,000 computing hours) takes only a few of minutes in a desktop computer with a 11th Gen Intel i7-11700F@2.50GHz processor.

The trained ANN provides an excellent estimation of ε_{hot}. As an example, Fig. 7 shows the results comparison of the values obtained with the ANN (lines) and MC simulations (symbols) in cases which were not included in the training set (different applied voltages and doping levels, for κ_r=3 and T=300, 400 and 500 K).

Fig. 9 represents the values of the breakdown voltage, V_B, as a function of T, N_D and κ_r estimated with the ANN model as the bias for which ε_{hot}=3.5 eV. To confirm that the ANN model is able to predict the voltages from which impact ionization becomes significant, in Fig. 10 we present the ionization rate obtained with a MC simulation considering N_D=0.8×10^{18} cm^{-3}, κ_r=6 and T=500 K. The applied voltage is 32.3 V, which is the voltage predicted by the ANN for V_B. As it can be observed, the MC results confirm the presence of a relevant number of impact ionizations in the hotspot area below the GaN-doped layer.

As a general trend, the results of Fig. 9 indicate that in order to achieve larger values of V_B (the limit for safe operation of the device from the point of view of breakdown induced by impact ionizations), it would be necessary to use low doping values for the GaN-doped layer and passivate the trenches with a dielectric with high permittivity. The temperature is a less critical factor, although higher temperatures favor larger values of V_B. If we plan to use these devices to fabricate high power sources for the THz range different constrictions are imposed by the fact that Gunn oscillations are more easily obtained with high values of N_D (the threshold voltage for the onset of the oscillations, V_{th}, decreases) [21]. For high doping values, higher than 2×10^{18} cm^{-3}, V_B is in the 19-24 V range, while at low doping values, high T and high κ_r values in the 40-45 V range could be reached. Since V_{th} is in the same voltage range [17], [21], there is a tradeoff between high V_B and low V_{th} in order to choose the optimum epilayer for the optimization of the design of the planar Gunn diodes. This side-effect cannot be considered as a spurious event: on the contrary, this can play a major role in the onset of a breakdown of the devices if the voltages surpass the critical limit. This is important in the context of top-view simulations of PGDs, that would not capture this phenomenon. Moreover, if one focuses on the extraction of the value of V_B only, instead than in the precise calculation of ε_{hot} for the whole voltage range, the number of MC simulations needed for the training can be significantly reduced by limiting the bias to a range about 15-45 V.

IV. Conclusions

A study of the critical voltage for the appearance of impact ionization processes in the buffer of planar Gunn diodes has been developed by combining MC simulations and a deep learning model. Front-view simulations allow capturing current leakage phenomena that are not observable by means of top-view models. MC simulations have evidenced that a high field hotspot below the GaN-doped region, at the corner of the etched trench on the anode side, leads to the appearance of highly energetic carriers out of the main transport region which can trigger impact ionization phenomena.

From a set of MC simulations, an ANN was trained and used to predict the critical voltages from which operation of the devices could not be safe due to impact ionization phenomena. The model accurately reproduces the dependence of the energy of the carriers at the high-field hotspot, and allows to correctly determine the voltage at which impact ionization becomes significant (eventually leading to device failure).

The results show that to extend the operability range of the diodes, a high permittivity of the isolating dielectric and a low doping of the GaN-doped active layer are recommended. In this way, voltages up to 45 V could be applied. This low doping can make difficult the generation of Gunn oscillations and, the selection of the epilayer features for the optimization of the design of planar Gunn diodes must be made considering this limitation. Consequently, a tradeoff between high breakdown voltages and low threshold biases to achieve high frequency oscillations must be adopted.

The combined approach presented here has the capability of capturing complex electronic transport features (hot electrons in secondary transport pathways) and providing an efficient prediction of potential device breakdown, thus helping to establish the safe operation conditions for the devices with a less time-consuming tool. This approach could be extended to help with the design of other high-power devices such as SiC or GaN HEMTs or Schottky barrier diodes, whose failure mechanisms are also triggered by impact ionization processes.

REFERENCES

[1] G. P. Gallerano and S. Biedron, "Overview of terahertz radiation sources," in *Proceedings of the 2004 FEL Conference,* 2004.

[2] F. Aniel et al, "Terahertz electronic devices," in Springer Handbook of Semiconductor Devices, M. Rudan, R. Brunetti and S. Reggiani, Eds. 2023, Available: https://doi.org/10.1007/978-3-030-79827-7_22. DOI: 10.1007/978-3-030-79827-7_22.

[3] J. V. Siles and J. Grajal, "Physics-based design and optimization of Schottky diode frequency multipliers for terahertz applications," *IEEE Trans. Microwave Theory Tech.,* vol. 58, *(7),* pp. 1933-1942, 2010.

[4] B. Alderman *et al*, "High power frequency multipliers to 330 GHz," in *The 5th European Microwave Integrated Circuits Conference,* 2010.

[5] H. Eisele, "State of the art and future of electronic sources at terahertz frequencies," *Electron. Lett.,* vol. 46, *(26),* pp. 8-11, 2010.

[6] A. Khalid *et al*, "Terahertz oscillations in an In0. 53Ga0. 47As submicron planar Gunn diode," *J. Appl. Phys.,* vol. 115, *(11),* pp. 114502, 2014.

[7] E. Alekseev and D. Pavlidis, "Large-signal microwave performance of GaN-based NDR diode oscillators," *Solid-State Electronics,* vol. 44, *(6),* pp. 941-947, 2000.

[8] R. F. Macpherson, G. M. Dunn and N. J. Pilgrim, "Simulation of gallium nitride Gunn diodes at various doping levels and temperatures for frequencies up to 300 GHz by Monte Carlo simulation, and incorporating the effects of thermal heating," *Semiconductor Science and Technology,* vol. 23, *(5),* pp. 055005, 2008.

[9] C. Sevik and C. Bulutay, "Gunn oscillations in GaN channels," *Semiconductor Science and Technology,* vol. 19, *(4),* pp. S188, 2004.

[10] S. García *et al*, "Comparative Monte Carlo analysis of InP-and GaN-based Gunn diodes," *J. Appl. Phys.,* vol. 115, *(4),* pp. 044510, 2014.

[11] S. Garcia *et al*, "Numerical study of sub-millimeter Gunn oscillations in InP and GaN vertical diodes: Dependence on bias, doping, and length," *J. Appl. Phys.,* vol. 114, *(7),* pp. 074503, 2013.

[12] W. Z. Lee *et al*, "Monte Carlo evaluation of GaN THz Gunn diodes," *Semiconductor Science and Technology,* 2021.
[13] A. S. Hajo *et al*, "Reliable GaN-based THz Gunn diodes with side-contact and field-plate technologies," *IEEE Access,* vol. 8, pp. 84116-84122, 2020.
[14] O. Yilmazoglu *et al*, "First observation of bias oscillations in GaN Gunn diodes on GaN substrate," *IEEE Trans. Electron Devices,* vol. 55, *(6),* pp. 1563-1567, 2008.
[15] O. Yilmazoglu *et al*, "Measured negative differential resistivity for GaN Gunn diodes on GaN substrate," *Electron. Lett.,* vol. 43, *(8),* pp. 480-482, 2007.
[16] K. Y. Xu, G. Wang and A. M. Song, "Gunn oscillations in a self-switching nanodiode," *Appl. Phys. Lett.,* vol. 93, *(23),* pp. 233506, 2008.
[17] J. Millithaler *et al*, "Optimized V-shape design of GaN nanodiodes for the generation of Gunn oscillations," *Appl. Phys. Lett.,* vol. 104, *(7),* pp. 073509, 2014.
[18] J. Mateos *et al*, "Design and fabrication of planar gunn nanodiodes based on doped GaN," in *2019 IEEE Asia-Pacific Microwave Conference (APMC),* 2019.
[19] S. García-Sánchez *et al*, "Non-linear thermal resistance model for the simulation of high power GaN-based devices," *Semiconductor Science and Technology,* vol. 36, *(5),* pp. 055002, 2021.
[20] M. Agrawal *et al*, "GaN-based SSD structure for THz applications," in *2019 IEEE Asia-Pacific Microwave Conference (APMC),* 2019.
[21] S. Garcia-Sanchez *et al*, "Optimization of the Epilayer Design for the Fabrication of Doped GaN Planar Gunn Diodes," *IEEE Trans. Electron Devices,* vol. 69, *(2),* pp. 514-520, 2021.
[22] S. García-Sánchez *et al*, "On the practical limitations for the generation of Gunn oscillations in highly doped GaN diodes," *Submitted Paper - February 2023.*
[23] K. Mukherjee *et al*, "Understanding the Leakage Mechanisms and Breakdown Limits of Vertical GaN-on-Si p+n−n Diodes: The Road to Reliable Vertical MOSFETs," *Micromachines,* vol. 12, *(4),* 2021. DOI: 10.3390/mi12040445.
[24] J. Chen *et al*, "Determination of the leakage current transport mechanisms in quasi-vertical GaN–on–Si Schottky barrier diodes (SBDs) at low and high reverse biases and varied temperatures," *Applied Physics Express,* vol. 14, *(10),* pp. 104002, 2021. Available: https://dx.doi.org/10.35848/1882-0786/ac2260. DOI: 10.35848/1882-0786/ac2260.
[25] M. A. Stošović and V. Litovski, "Application of Artificial Neural Networks in Electronics," *Electronics,* vol. 21, *(2),* pp. 87-94, 2017.
[26] C. Jeong *et al*, "Bridging TCAD and AI: Its Application to Semiconductor Design," *IEEE Transactions on Electron Devices,* vol. 68, *(11),* pp. 5364-5371, 2021. DOI: 10.1109/TED.2021.3093844.
[27] E. Kim *et al*, "Fault Detection and Diagnosis Using Self-Attentive Convolutional Neural Networks for Variable-Length Sensor Data in Semiconductor Manufacturing," *IEEE Transactions on Semiconductor Manufacturing,* vol. 32, *(3),* pp. 302-309, 2019. DOI: 10.1109/TSM.2019.2917521.
[28] J. Mateos *et al*, "Monte Carlo simulator for the design optimization of low-noise HEMTs," *IEEE Trans. Electron Devices,* vol. 47, *(10),* pp. 1950-1956, 2000.
[29] O. Madelung, *Semiconductors: Data Handbook.* 2004.
[30] M. V. Fischetti, "Monte Carlo simulation of transport in technologically significant semiconductors of the diamond and zinc-blende structures. I. Homogeneous transport," *IEEE Trans. Electron Devices,* vol. 38, *(3),* pp. 634-649, 1991.
[31] F. Bertazzi, M. Moresco and E. Bellotti, "Theory of high field carrier transport and impact ionization in wurtzite GaN. Part I: A full band Monte Carlo model," *J. Appl. Phys.,* vol. 106, *(6),* pp. 063718, 2009.
[32] B. G. Vasallo *et al*, "Monte Carlo study of kink effect in short-channel InAlAs/InGaAs high electron mobility transistors," *J. Appl. Phys.,* vol. 94, *(6),* pp. 4096-4101, 2003.
[33] Z. Zheng, Y. Mai and G. Wang, "Monte Carlo study of device characteristics of GaN-based avalanche photodiode devices," *J. Appl. Phys.,* vol. 106, *(2),* pp. 023716, 2009.
[34] S. Chen and G. Wang, "High-field properties of carrier transport in bulk wurtzite GaN: A Monte Carlo perspective," *J. Appl. Phys.,* vol. 103, *(2),* pp. 023703, 2008.
[35] I. Iñiguez-De-La-Torre *et al*, "Influence of the surface charge on the operation of ballistic T-branch junctions: a self-consistent model for Monte Carlo simulations," *Semiconductor Science and Technology,* vol. 22, *(6),* pp. 663, 2007.
[36] A. Tanaka *et al*, "Structural and electrical characterization of thick GaN layers on Si, GaN, and engineered substrates," *J. Appl. Phys.,* vol. 125, *(8),* pp. 082517, 2019. Available: https://doi.org/10.1063/1.5049393. DOI: 10.1063/1.5049393.
[37] G. Panchal *et al*, "Behaviour analysis of multilayer perceptrons with multiple hidden neurons and hidden layers," *International Journal of Computer Theory and Engineering,* vol. 3, *(2),* pp. 332-337, 2011.
[38] J. Heaton, *Introduction to Neural Networks with Java.* 2008.
[39] *The Comprehensive R Archive Network*. Available: http://cran.r-project.org.
[40] A. D. Anastasiadis, G. D. Magoulas and M. N. Vrahatis, "New globally convergent training scheme based on the resilient propagation algorithm," *Neurocomputing,* vol. 64, pp. 253-270, 2005.
[41] M. Riedmiller and H. Braun, "A direct adaptive method for faster backpropagation learning: The RPROP algorithm," in *IEEE International Conference on Neural Networks,* 1993.
[42] J. Qi *et al*, "On mean absolute error for deep neural network based vector-to-vector regression," *IEEE Signal Process. Lett.,* vol. 27, pp. 1485-1489, 2020.